Journal of Applied Fluid Mechanics, Vol. 17, No. 1, pp. 284-296, 2024.
Available online at www.jafmonline.net, ISSN 1735-3572, EISSN 1735-3645.
https://doi.org/10.47176/jafm.17.1.1917

Modeling Multiphase Debris Floods Down Straight and Meandering Channels

P. Kattel[1], C. N. Tiwari[1,2], B. R. Dangol[2,3] and J. Kafle[2†]

[1] *Department of Mathematics, Tri-Chandra Multiple Campus, Tribhuvan University, Kathmandu, Nepal*
[2] *Central Department of Mathematics, Tribhuvan University, Kathmandu, Nepal*
[3] *Department of Mathematics, Patan Multiple Campus, Tribhuvan University, Lalitpur, Nepal*

†*Corresponding Author Email: jeevan.kafle@cdmathtu.edu.np*

ABSTRACT

Natural debris floods travel in straight and meandering courses. The flow behaviour greatly depends on the volume fractions of solid and fluid, as well as on their dynamic interactions with the channel geometry. For the quasi three-dimensional simulations of flow dynamics and mass transport of these floods through meandering and straight channels, we employ a two-phase debris flow model to carry out simulations for debris floods within straight and sine-generated meandering channels of different amplitudes. The results for different sinuous meandering paths are compared with that in the straight one in terms of phase velocity, downslope advection and dispersion, depths of the maxima, deposition of mass, position of front and rear parts of the solid and fluid phases, and also the flow dynamics out of the conduits. The results reveal the slowing of the flow and increase of momentary deposition of the mixture mass in the vicinity of the bends along with the increasing sinuosity. The numerical experiments are useful to better understand the dynamics of debris floods down meandering channels as seen in the natural paths of the rivers as well as already existing channels like episodic rivers in hilly regions. The results can be extended to propose some appropriate mitigation strategies.

Article History

Received April 17, 2023
Revised August 23, 2023
Accepted August 28, 2023
Available online November 1, 2023

Keywords:

Two-phase mass flow
Debris flood
Meandering channel
Sinuosity
Flow within Conduits

1. INTRODUCTION

Channels define the course of the (river) flow confined by banks. River channel may vary in width, depth and shape. Flow depends on its velocity, volume and discharge, slope or steepness of the river channel, and erosion and sedimentation of the materials from banks and beds. These river characteristics contribute to adjust the channel to change, shaping the river channel and creating various landforms, such as river valleys, meanders, and deltas (Montgomery & Buffington, 1998; Bogoni et al., 2017). The sediment concentration in a river water flow in the normal situation is very low, and the sediments play no significant influence in the flow dynamics in the short run, whereas the amount of silt, clay, sand and boulder in a flow mixture is sufficient to substantially alter fluid dynamics and transport mechanisms. A flood occurs when the discharge of water and sediment in the channel exceeds its capacity, and the river banks are overflowed (Montgomery & Buffington, 1998). Most often, water floods transport fine sediments with low concentration and has little impact on the flow behaviour. However, high-discharge debris floods may transport high sediment concentrations, and this has high influence on the mechanics and behavior of the flow (Pierson, 2005a). The relative velocities of constituent phases (water and sediments) within debris flow or flood is small. Both solid and fluid forces, their interactions and continuous deformations play significant role in the flow dynamics (Coussot & Meunier, 1996; Coussot & Ancey, 1999; Delannay et al., 2017). A debris flood in a mountain river usually occurs as a sudden and temporary flow at a speed 10 m/s or even more. Due to sharp rise in water level with mixture of sediment, a debris flood often moves in individual surges or waves. This makes a debris flood different from an ordinary flood (Pierson, 2005b; Iverson & George, 2014; Kattel et al., 2018). These large scale mass movements that propelled by the gravitational acceleration in combination with the pressure and topographic gradients in mountainous areas are highly destructive to infrastructure and human lives (Iverson, 1997; Pudasaini, 2012).

Path of the river is not always straight. It is common for a river to change its course in nature due to the localized distortion in bending conduits and blockage of

Fig. 1 A meandering river (Duan & Julian, 2005)

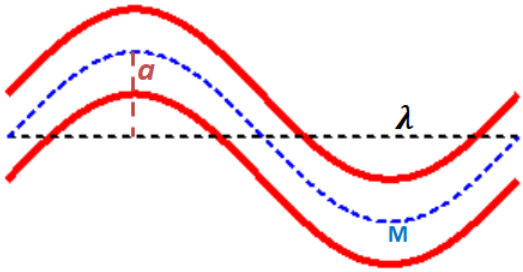

Fig. 2 A sine-generated meandering channel (Hagerman & Williams, 2000)

the course by the large boulders (Leopold & Wolman, 1960). In order to sustain the river condition, it is crucial to understand the hydraulics and hydrology of streams that characterize the river (Yong et al., 2018). There are three most common channel patterns, namely, straight (low or no sinuosity), braided (network of channels or multiple-thread channels that split and rejoin) and meandering (bended or curved). Meandering river channels may have medium to high sinuosity and generally have almost constant width. The meandering channels are different from the straight ones by their sinuously winding course (Murray and Paola 1994). The channel pattern may alter along the length of a river as it flows, particularly during flood stage (Montgomery & Buffington, 1998). Meandering rivers are characterized by the recurrent pattern of the opposing processes of lateral migration and cut off formations (Kopera, 2014; Parker et al., 1983). Meandering of a river or other watercourse over its length is commonly measured by its sinuosity, $S = \frac{M}{\lambda}$, where M is the arc length of the flow path between two points and λ is the shortest distance between them, called linear wave length (see Fig. 2) (Stolum, 1996; Hagerman & Williams, 2000; Mohamad et al., 2015). A channel is meandering with moderate sinuosity if S is less than or equal to 1.5, and that with active sinuosity if $S > 1.5$. Theoretically, sinuosity has no maximum value. A complete sinuous curve has a sinuosity of around 6, whereas it ranges between 7 and 40 while tending to form the oxbow lake due to sharp meandering (Stolum, 1996). In fact, a meander shape can be mathematically modeled in various ways. Examples include sine, parabolic, circular and sine generated curves (Langbein & Leopold, 1966).

Meandering rivers are found to be studied in geomorphological and fluid dynamical approaches. The geomorphological approach includes fundamental field studies (Friedkin, 1945; Kinoshita, 1961) and laboratory experiments (Rozovskii, 1957; Zimmerman & Kennedy, 1978) to provide empirical relationships on meanders and river bed formations including flow patterns, sediment movement, erosion, and deposition. If the valley slope is low and stable, the channel-incision occurs mainly vertically so as to inherit a pre-existing sinuous pattern. If the regional slope steepens, the meandering of channel accompanies the vertical incision. The steepening regional slope amplifies sinuosity, especially when the flow is confined (Dente et al., 2021). The fluid mechanical approach, on the other hand, has concentrated on the modeling of the physical process to govern the dynamics of the meandering flow (Camporeale et al., 2002).

The pioneer work of Ikeda & Nishimura (1986) greatly devoted on the development of credible theoretical models for meander simulations. In particular, this is the first model to capture the evolution of single reach of river bends with a linkage of the flow field and the erosion rate (Gu et al., 2016). Yong et al. (2018) experimentally obtained different interesting erosion and deposition patterns and meandering phenomena. For a river channel, Crosato (2008) developed some special methods to calculate the number of bars, which can predict the river channel type: meandering and braiding. Gu et al. (2016) performed some experiments and also simulated the flow pattern and evolution of meandering for differently sinuous channels employing the linear and nonlinear hydrodynamic models which accounts for the nonlinear interactions between secondary flow and main flow. Both the models reveal the similar results for the channels with lower sinuosity but they vary for the larger sinuosity. Motta et al. (2012) used physics-based streambank erosion formulations to calculate rates of meander migration.

Numerous studies on the mathematical models of debris flows/floods are primarily concentrated on single-phase (Bagnold, 1954; Chen, 1988; Takahasi, 2007) and solid-fluid mixtures (Iverson, 1997, 2003). However, in nature, interaction between the grains and the surrounding fluid plays a crucial role in the flow dynamics and such gravitational mass flows are three dimensional in nature (Cassar et al., 2005). Single-phase models cannot well describe complex interactions between the fluid and solid phases; however, they are much easier to parameterize than multiphase models. Moreover, three-dimensional modeling of these rapidly propagating flows takes a large computational effort. To overcome it with a good accuracy, depth integrated models are applied (Pastor et al., 2018). Using two-phase mass flow model including ambient drag, Kattel et al. (2016) performed numerical experiments to simulate glacial lake outburst floods (GLOFs) in different idealized situations and revealed different dynamics of solid particles and viscous fluid. Kattel et al. (2018)

further performed different computational experiments and presented results related to the detailed dynamical interactions of the debris mixture with stationary obstacles of distinct orientations, numbers, sizes and spacing placed on a slope running out into a horizontal plane. Kattel and Tuladhar (2018) simulated the debris flow through lateral converging shear walls to study the relation between the flow obstruction and the contraction ratios. In some cases of these numerical experiments, flows pass through non-meandering channels. Numerous mathematical and empirical advancements have been made in the study of debris floods and flows down an incline. However, numerical experiments in two phases and three dimensions are still lacking, especially for meandering channels. Duan (2004) developed two-dimensional numerical model suitable for meandering channels to simulate flow hydrodynamics and mass transport, and compared the results with a laboratory experiment for the flow in a sine generated channel. Duan and Julien (2005) modeled and simulated the inception and development of channel meandering process.

River meandering is a very common natural phenomenon. (Coz et al., 2010). Many episodic floods occur in pre-existing meandering channels. The more accurate study of flow dynamics in meandering channels are needed for the safety of the people and infrastructures. Especially while constructing roads at the side of the river bank, the study is even more important. So, using the physics-based two phase mass flow model and effective simulation techniques, we further advance to investigate the dynamics and the devastation potential of a debris flood in generic meandering channels with varied sinuosities. The floods in mountain gulley and pre-existing channels of episodic rivers are even more hazardous due to steep slopes. This work mainly focuses on some dynamical aspects of the simulations of two-phase debris floods akin to those in pre-existing non-deformable channels of episodic rivers with different sinuosity by using the two-phase mass flow model (Pudasaini, 2012) so as to obtain the explicit geometric evolution of the separate solid and fluid phases.

2. PHYSICAL-MATHEMATICAL MODEL

To simulate debris flood down straight and meandering conduits, we use the two-phase mass flow model (Pudasaini, 2012), where the phases (fluid and solid particles) are described by their material properties: viscosity η_f, density of the viscous fluid ρ_f and stress distribution (isotropic) for fluid; angles of the basal friction δ, internal friction ϕ, material density ρ_s, and a stress distribution (anisotropic) through the lateral earth pressure coefficient K for solid. The model constitutes a system of mass and momentum balances as highly non-linear parabolic-hyperbolic partial differential equations, which are mentioned below in (1)-(6). In these equations, the spatial coordinates x, y and z are along the directions of downslope, cross-slope and the normal to the flow surface, respectively; t is the temporal coordinate; g^x, g^y and g^z are the components of acceleration due to gravity in the respective directions. The subscripts f and s denote the fluid phase and the solid phase with respective depth-averaged velocity components $u_f = (u_f, v_f)$ and $u_s = (u_s, v_s)$ in x and y directions. The depth of the mixture is h, α_s and α_f are respective fractions of solid and fluid volume so that $\alpha_f + \alpha_s = 1$.

$$\frac{\partial}{\partial t}(\alpha_s h) + \frac{\partial}{\partial x}(\alpha_s h u_s) + \frac{\partial}{\partial y}(\alpha_s h v_s) = 0 \tag{1}$$

$$\frac{\partial}{\partial t}(\alpha_f h) + \frac{\partial}{\partial x}(\alpha_f h u_f) + \frac{\partial}{\partial y}(\alpha_f h v_f) = 0 \tag{2}$$

$$\frac{\partial}{\partial t}\left[\alpha_s h\left(u_s - \gamma\mathcal{C}\left(u_f - u_s\right)\right)\right] + \frac{\partial}{\partial x}\left[\alpha_s h\left(u_s^2 - \gamma\mathcal{C}\left(u_f^2 - u_s^2\right) + \beta_{x_s}\frac{h}{2}\right)\right] + \frac{\partial}{\partial y}\left[\alpha_s h\left(u_s v_s - \gamma\mathcal{C}\left(u_f v_f - u_s v_s\right)\right)\right] = hS_{x_s} \tag{3}$$

$$\frac{\partial}{\partial t}\left[\alpha_s h\left(v_s - \gamma\mathcal{C}\left(v_f - v_s\right)\right)\right] + \frac{\partial}{\partial x}\left[\alpha_s h\left(u_s v_s - \gamma\mathcal{C}\left(u_f v_f - u_s v_s\right)\right)\right] + \frac{\partial}{\partial y}\left[\alpha_s h\left(v_s^2 - \gamma\mathcal{C}\left(v_f^2 - v_s^2\right) + \beta_{y_s}\frac{h}{2}\right)\right] = hS_{y_s} \tag{4}$$

$$\frac{\partial}{\partial t}\left[\alpha_f h\left(u_f + \frac{\alpha_s}{\alpha_f}\mathcal{C}\left(u_f - u_s\right)\right)\right] + \frac{\partial}{\partial x}\left[\alpha_f h\left(u_f^2 + \frac{\alpha_s}{\alpha_f}\mathcal{C}\left(u_f^2 - u_s^2\right)\right) + \beta_{x_f}\frac{h}{2}\right] + \frac{\partial}{\partial y}\left[\alpha_f h\left(u_f v_f + \frac{\alpha_s}{\alpha_f}\mathcal{C}\left(u_f v_f - u_s v_s\right)\right)\right] = hS_{x_f} \tag{5}$$

$$\frac{\partial}{\partial t}\left[\alpha_f h\left(v_f + \frac{\alpha_s}{\alpha_f}\mathcal{C}\left(v_f - v_s\right)\right)\right] + \frac{\partial}{\partial x}\left[\alpha_f h\left(u_f v_f + \frac{\alpha_s}{\alpha_f}\mathcal{C}\left(u_f v_f - u_s v_s\right)\right)\right] + \frac{\partial}{\partial y}\left[\alpha_f h\left(v_f^2 + \frac{\alpha_s}{\alpha_f}\mathcal{C}\left(v_f^2 - v_s^2\right) + \beta_{y_f}\frac{h}{2}\right)\right] = hS_{y_f}, \tag{6}$$

where

$$\beta_{x_s} = \varepsilon K_x p_{b_s}, \beta_{y_s} = \varepsilon K_y p_{b_s}, \beta_{x_f} = \beta_{y_f} = \varepsilon p_{b_f}, \quad p_{b_f} = -g^z, \qquad p_{b_s} = (1-\gamma)p_{b_f}.$$

Among these equations, (1) and (2) are the depth-averaged mass conservation for solid and fluid phases respectively, and the last four equations are the depth averaged momentum conservation for solid (3)-(4) and fluid (5)-(6), in *x*- and *y*-directions respectively. The right hand sides of the last four momentum conservation equations are the source terms given by:

$$S_{x_s} = \alpha_s\left[g^x - \frac{u_s}{|\boldsymbol{u_s}|}\tan\delta\, P_{b_s} - \varepsilon P_{b_s}\frac{\partial b}{\partial x}\right] - \epsilon\alpha_s\gamma P_{b_f}\left[\frac{\partial h}{\partial x} + \frac{\partial b}{\partial x}\right] + C_{DG}\left(u_f - u_s\right)\left|\boldsymbol{u_f} - \boldsymbol{u_s}\right|^{j-1} \tag{7}$$

$$S_{y_s} = \alpha_s\left[g^y - \frac{v_s}{|\boldsymbol{u_s}|}\tan\delta\, P_{b_s} - \varepsilon P_{b_s}\frac{\partial b}{\partial y}\right] -$$

$$\varepsilon\alpha_s\gamma P_{b_f}\left[\frac{\partial h}{\partial y}+\frac{\partial b}{\partial y}\right]+C_{DG}\left(v_f-v_s\right)\left|\boldsymbol{u_f}-\boldsymbol{u_s}\right|^{j-1} \quad (8)$$

$$S_{x_f}=\alpha_f\left[g^x-\varepsilon\left[\frac{1}{h}\frac{\partial}{\partial x}\left(\frac{h^2}{2}P_{b_f}\right)+P_{b_f}\frac{\partial b}{\partial x}+\right.\right.$$
$$-\frac{1}{\alpha_f N_R}\left\{2\frac{\partial^2 u_f}{\partial x^2}+\frac{\partial^2 v_f}{dy\,dx}+\frac{\partial^2 u_f}{\partial y^2}-\frac{\chi u_f}{\varepsilon^2 h^2}\right\}$$
$$+\frac{1}{\alpha_f N_{R_A}}\left\{2\frac{\partial}{\partial x}\left(\frac{\partial\alpha_s}{\partial x}\left(u_f-u_s\right)\right)+\right.$$
$$\left.\left.\frac{\partial}{\partial y}\left(\frac{\partial\alpha_s}{\partial x}\left(v_f-v_s\right)+\frac{\partial\alpha_s}{\partial y}\left(u_f-u_s\right)\right)\right]-\right.$$
$$\left.\frac{\xi\alpha_s(u_f-u_s)}{\varepsilon^2\alpha_f H_{R_A}h^2}\right]+C_{DG}\left(u_f-u_s\right)\left|\boldsymbol{u_f}-\boldsymbol{u_s}\right|^{j-1} \quad (9)$$

$$S_{y_f}=\alpha_f\left[g^y-\varepsilon\left[\frac{1}{h}\frac{\partial}{\partial y}\left(\frac{h^2}{2}P_{b_f}\right)+P_{b_f}\frac{\partial b}{\partial y}-\right.\right.$$
$$\frac{1}{\alpha_f N_R}\left\{2\frac{\partial^2 v_f}{\partial y^2}+\frac{\partial^2 u_f}{dx\,dy}+\frac{\partial^2 v_f}{\partial x^2}-\frac{\chi u_f}{\varepsilon^2 h^2}\right\}$$
$$+\frac{1}{\alpha_f N_{R_A}}\left\{2\frac{\partial}{\partial y}\left(\frac{\partial\alpha_s}{\partial y}\left(v_f-v_s\right)\right)+\frac{\partial}{\partial x}\left(\frac{\partial\alpha_s}{\partial y}\right.\right.$$
$$\left.\left.\left(u_f-u_s\right)\frac{\partial\alpha_s}{\partial x}\left(v_f-v_s\right)\right)\right\}-\left.\frac{\xi\alpha_s\left(v_f-v_s\right)}{\varepsilon^2\alpha_f N_{R_A}h^2}\right]\Bigg]$$
$$+C_{DG}\left(v_f-v_s\right)\left|\boldsymbol{u_f}-\boldsymbol{u_s}\right|^{j-1}. \quad (10)$$

In these source terms, some parameters are given by:

$$C_{DG}=\frac{\alpha_s\alpha_f(1-\gamma)}{\left[\varepsilon\mathcal{U}_T\{\mathcal{P}\mathcal{F}(Pe_p)+(1-\mathcal{P})\mathcal{G}(Re_p)\}\right]^j}$$
$$\mathcal{F}=\frac{\gamma}{180}\left(\frac{\alpha_f}{\alpha_s}\right)^3 Re_p, \mathcal{G}=\alpha_f^{M(Re_p)-1}, \gamma=\frac{\rho_f}{\rho_s}$$
$$\mathcal{C}=\frac{1}{2}\left(\frac{1+2\alpha_s}{\alpha_f}\right), \qquad Re_p=\frac{\rho_f d\mathcal{U}_T}{\eta_f}$$
$$N_R=\frac{\sqrt{gL}H\rho_f}{\alpha_f\eta_f}, \qquad N_{R_A}=\frac{\sqrt{gL}H\rho_f}{\mathcal{A}\eta_f}. \quad (11)$$

To further explain the terms involved, the aspect ratio is $\epsilon=\frac{H}{L}$, where H and L are the typical depth and the length of the flow. The coefficient $\mu=\tan\delta$ measures the basal friction, C_{DG} is the coefficient of the generalized drag due to the difference of the phase velocities, which has been interpolated by a parameter $\mathcal{P}\in[0,1]$ as a linear combination of the solid-like drag ($\mathcal{G}$) and fluid-like drag ($\mathcal{F}$). The index $j=1$ describes the linear drag and (laminar-type, at low velocity), whereas $j=2$ describes the quadratic (turbulent-type, at high velocity) drag. The terminal velocity of a freely falling particle in fluid is denoted by $\mathcal{U}_T$. The ratio of the fluid-density to the solid-density is γ, the function *M* depends on the particle Reynolds number (Re_p), vertical shearing of fluid velocity is included by χ, and ξ incorporates various distributions of α_s. The interfacial fluid mobility is $\mathcal{A}$. The quasi-Reynolds number associated with the classical Newtonian stress is N_R, whereas the mobility-Reynolds number associated with the enhanced non-Newtonian fluid viscous stress if N_{R_A}. The virtual mass coefficient $\mathcal{C}$ appears at the inertial terms when there is relative acceleration between the phases. The novel virtual mass coefficient for multiphase mass flow can be found in Kattel et al. (2021).

3. SIMULATION SET-UP

3.1 Flow Channel, Conduits and Release Mass

For the simulation, the flow surface is in the shape of a rectangle with computational domain in $[-50,390]\times[-200,200]$ m which is an inclined surface in downward direction with a slope of 45^o. Sinuous path of the debris flood is generated by the sine curves as

$$y_l=a\sin\left(c(x-x_0)\right)-\frac{b}{2} \quad (12)$$

$$y_u=a\sin\left(c(x-x_0)\right)+\frac{b}{2}, \quad (13)$$

where a denotes the amplitude of the sine generated channels that begins from the position $x=x_0$ with uniform breadth b and $c=0.06733$. We put amplitude $a=0$ and $b=20$ for straight channel (sinuosity $=1$) of uniform width 20 m. We choose $x_0=50$ and $b=20$ for the continuous sinuous channel of uniform width 20 m from $x=x_0=50$ m to $x=x_r=144$ m and the conduits are almost vertical with inclination 88.7^o that confine the flow. In three different initial conditions for simulations, the conduits have a straight boundaries and sinuous curves with amplitudes $a=15$ and $a=30$ m. Within the mentioned computational domain, here we present some basic simulations of a two phase debris flood down in

1. straight channel with domain $[0,200]\times[-10,10]$ m (Fig. 3 A).
2. straight channel at $[0,50]\times[-10,10]$ m followed by a sinuous meandering channel with amplitude $a=15$ m at $[50,144]\times[y_l,\,y_u]$ m and ends with a straight channel with domain $[144,200]\times[-10,10]$ m (Fig. 3 B).
3. straight channel that span within $[0,50]\times[-10,10]$ m followed by a sinuous meandering channel with amplitude $a=30$ m within $[50,144]\times[y_l,\,y_u]$ m and finally ends with a straight channel with domain $[144,200]\times[-10,10]$ m (Fig. 3 C).

For $200\text{ m}\le x\le 390$ m, as there is no any conduit, the flow is subjected to an undisturbed flow. The mixture can flow freely under the influence of momentum and gravity when it exits the channel. The initial mass of deformable debris is in the shape of a triangular wedge $[0,50]\times[-10,10]$ m as shown in the initial setup (Fig. 3 A). So as to make the flow akin to a natural debris flood, the release mass is a uniform mixture of 20% solid and 80% fluid as sediment

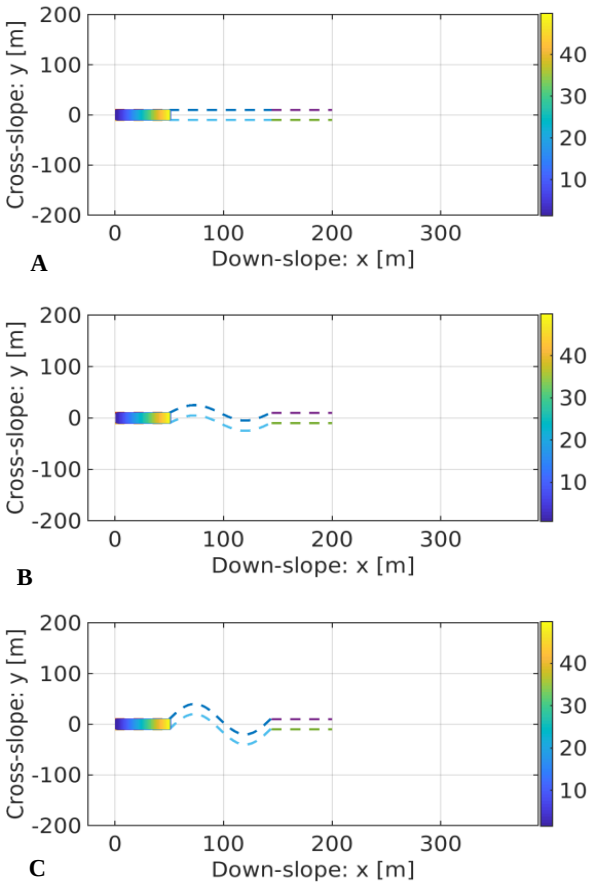

Fig. 3 Bird eye view of total initial mass configuration and flow channel: A: straight channel, B: sinuous channel with amplitude 15 m, C: amplitude 30 m

concentrations in natural debris floods range from 20 to 47% by volume (Wilford et al., 2004). However, the solid concentration in debris flow generally ranges from 50 to 90 % (Coussot & Meunier, 1996). The numerical experiments are performed by releasing the debris mass that flow within a straight or sinuous meandering channel interacting with non-deformable vertical walls. The dynamic behaviour of the flow is influenced by the volume of the release mass, slope of the topography and concentration of the phases (Kafle et al., 2021, 2022, 2023) as well as the sinuosity of the meander. Here, the length of the curved river path is calculated as

$$M = \int_{\alpha}^{\beta} \sqrt{1 + \left(\frac{dy}{dx}\right)^2}\, dx,$$

where $x = \alpha$ and $x = \beta$ represent lower and upper bounds of the sinuous part of the river in downslope directions respectively (Fig. 2). When we take $a = 15$ m for the sinuous channel to denote the amplitude of 15 m (Fig. 3 B), the length of the curved river is calculated as

$$M = \int_{50}^{144} \sqrt{1 + a^2\, \lambda^2 \cos^2\big(\lambda(x-50)\big)}\, dx = 115.15 \text{ m}$$

so that the sinuosity is

$$S = \frac{M}{\lambda} = \frac{115.15}{144.2477 - 50} = 1.22$$

and the degree of meandering is moderate.

Similarly, for the channel with amplitude 30 m (Fig. 3 Right), we get $M = 159.6072$ and sinuosity is $S = \frac{M}{\lambda} = 1.6983$, indicating an active meandering.

For the straight channel (Fig. 3 Left), the sinuosity is 1.

3.2 Parameter Values and Numerical Method

For the numerical simulation purpose, we consider the volume fractions of the phases in the initial mixture are $\alpha_s = 0.2, \alpha_f = 0.8$. The nondimensional parameters chosen are taken as: $\delta = 15^{\circ}, \varphi = 35^{\circ}, \mathcal{U}_T = 1.0, Re_p = 1, \chi = 1, \xi = 0.5, C = 0.5, J = 1,$ $N_R = 3 \times 10^4$ and $N_{R_A} = 1000$.

The flow surface's inclination angle is $\zeta = 45^{\circ}$.

These parameter choices are dependent on the dynamics of two-phase subaerial and submarine mass flows, as described in Pudasaini (2012), Pudasaini and Krautblatter (2014), Kattel et al. (2016), and Kafle et al. (2016). The values can differ depending on the properties of the materials and flow situation. Gravitational mass flows may encounter barriers, and may show massive deformations during the flow and sudden changes in flow dynamical variables. We use the TVD-NOC (total variation diminishing non-oscillatory central) schemes (Tai et al., 2002) for numerical integration of the governing equations (1)-(6) in order to capture such complicated phenomenon.

4. SIMULATION RESULTS AND DISCUSSION

To simulate the natural debris floods along these channel geometries, the initial debris mass containing 20% solid and 80% fluid which is in the shape of a triangular wedge that triggers and flows in an inclined surface. We will conduct three sets of computational experiments for two-phase mass flow akin to debris flood in meandering channels using a two-phase mass flow model and high resolution numerical simulation techniques. The results of simulations for debris flood in straight and sinuous meandering conduits of different amplitudes are compared.

4.1 Debris Flood Down a Straight Channel

Using the aforementioned initial geometry and the parameters, we exhibit a reference simulation result for a flow akin to a debris flood down in a continuous straight channel. The time evolution ($t = 1 - 7$ s) of the total flood depth has been presented here in Fig. 4 (panels C). The colour bar in each panel and the colours in our contour plots correspond to the depths of the material. Initially at $t = 0$ s, overall depth of the mixture at the front of the release mass is 50 m in which contribution of solid is 10 m. As time elapses, flow quickly advects in the downslope due to pressure and gravity and the maxima of the mixture quickly shift from front to the

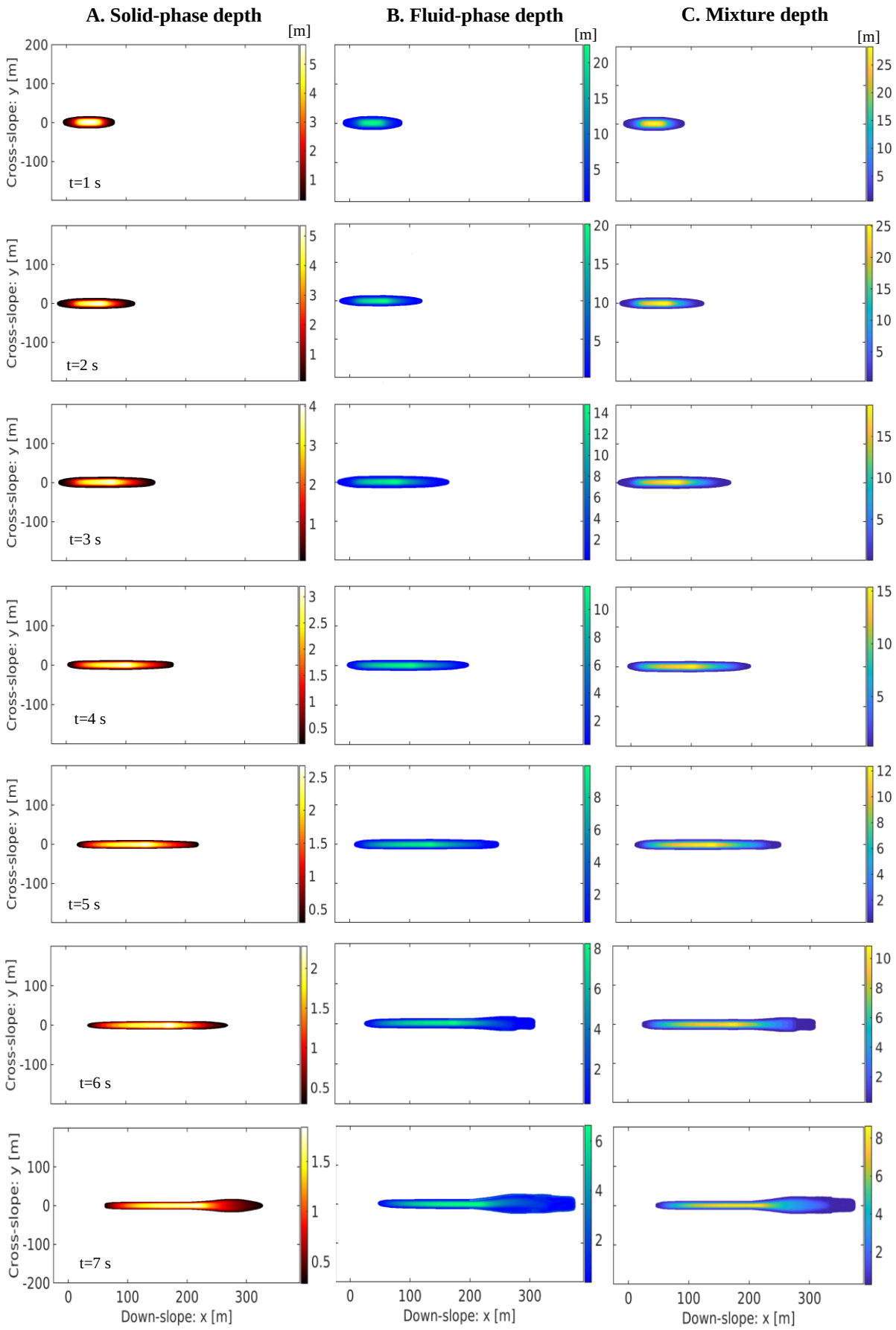

Fig. 4 Time and spatial evolution of the solid phase (panels A), fluid phase (panels B), and total debris (panels C) at t= 1, 2, 3, 4, 5, 6 and 7 s as the debris flood (0 m ≤ x ≤ 50 m) triggers and moves down along straight channel (0 m ≤ x ≤ 200 m), and as a free surface flow after x = 200 m. Elongated flow maxima are seen at the central part of the flowing mixture

middle ($t = 1$ s) (panel C). As the flow is confined by the lateral boundaries, the spreading in lateral direction is hindered and the flow is only pronounced along the downstream as time elapses. On the other hand, during $t = 1 - 3\ s$, back flow continues due to pressure gradient as there is no conduit at the rear part of the release mass. After $t = 4$ s, the effect ceases and due to the gravity, the front, middle and rear part all begin to advect substantially as time progresses. As the pressurized flowing mass at the middle and head obscured the flow of mass at the back, the rear part's advection along the downslope can only be substantially observed after $t = 4$ s. From $t = 2$ s onward, the flow maxima is gradually elongating at the middle position and then gradually shifting to the rear part when the mass exits the channel especially after $t = 6$ s. This indicates the momentary obstruction of the flow due to the narrow lateral boundaries relative to the mass. From $t = 5$ s onward, the flow begins to exit the conduits. As the flow is free from the lateral confinements, the frontal head of the flow shows spreading across and gets wider head, especially after $t = 6$ s. The total debris is further showing the tendency to advect downslope because of the existing momentum. When the mass exits the conduits, the maximum moves from middle to the rear part. It is because of the narrow lateral confinements which hinders the flow but the rear part is still advecting. The flow front almost reaches to the end of right to the surface at $t = 7$ s. The advantage of the two-phase mass flow model and our simulation techniques is that, we can explicitly show the evolution and the dynamics of the separate solid and fluid phases as well. Their separate evolution and the dynamics have been presented in the panels A and B of Fig. 4. The fluid phase only and the mixture both exhibit nearly identical geometrical evolutions as the concentration of fluid in the mixture exceeds the solid by a large margin. Fluid flows more quickly than the solid as the solid experiences the internal friction and the virtual mass force increases the kinetic force of the solid. At $t = 2, 3, 4, 5, 6$ and 7 s, the fronts of the fluid phase are located respectively at $x = 91$ m, $x = 124$ m, $x = 155$ m, $x = 200$ m, $x = 250$ m, $x = 309$ m and $x = 376$ m, whereas the heads of the solid phase are at $x = 88$ m, $x = 115$ m, $x = 145$ m, $x = 180$ m, $x = 225$ m, $x = 271$ m and $x = 325$ m, respectively. The solid starts to exit the conduits at $t = 5$ s, but the fluid does so already at $t = 4$ s because the fluid has a greater mobility. Lower density and material friction enable the fluid not only to advect quickly in downslope direction but also to spreads transversely. A remarkable crosswise dispersion in the fluid phase can be detected at $t = 6$ s but not in solid phase. However at $t = 7$ s, a marginally wider head caused by transverse shearing can be visible in contrast to a slightly dispersed head visible in solid at that time.

4.2 Debris Flood Down a Meandering Channel with Moderate Sinuosity

To simulate the debris flood along meandering conduits with moderate sinuosity of amplitude 15 m, we consider initial mass akin to debris flood in the form of a triangular wedge that triggers and moves down in an inclined slope. The evolution of the total flood for different times $t = 1$ s to $t = 7$ s has been presented here in panels C of Fig. 5. Similar to the flow in a straight conduits, pressure and gravity driven flow quickly advects on the downslope direction over time, shifting the mixture's maxima from the front to the middle. As the flow is channelized by the lateral meandering boundaries, meandering of the flow is more and more visible as time elapses. Similar to the flow at the straight channel, pressure gradient-induced reverse flow persists for $t = 1 - 3$ s because the pressure created by the momentarily obstruction due to narrow conduits at the entry to the channel causes the reverse flow (Tulapurkara et al., 1994) and only downslope advection of the rear part occurs after $t = 4$ s. After $t = 2$ s onwards, the flow maxima are seen at vicinity of the bends where the flow is interrupted momentarily. As we observed only an elongated maximum in the straight channel (Fig. 4), but dispersed maxima at the bends are seen with the moderately meandering conduits (Fig. 5). Consequently, unlike in the straight channel, the maximum flow depth does not suddenly drop after $t = 4$ s when the meandering is more apparent. The respective depths of the maxima are $19, 18, 15$ and 12 m (panels C of Fig. 5) in $t = 4$ s to $t = 7$ s, whereas they were $15, 12, 10, 8$ m (panels C of Fig. 4) in the straight channel. Flow begins to exit the conduits at $t = 4$ s in the straight channel, whereas it does at $t = 5\ s$ in Fig. 5 and the maxima of the mixture shifts to the bends at rear part. This shows the temporal reduction in the flow velocity due to the obstruction. The frontal head manifests expanding across and becoming wider as the flow is not hindered by lateral confinements.

The main body and the tails are showing meandering shape until $t = 7$ s. The flow reaches to only $x = 340$ m at $t = 7$ s in Fig. 5 but it has already reached at $x = 376$ m in the straight conduits (Fig. 4) because the obstruction in the bends to some extent controls the momentum of the flow. The separate evolution and the dynamics of the phases have been presented in the panels A and B of Fig. 5. At $t = 1\ s$, the solid and fluid both advect and the fronts begin to move down within the conduit walls. The meandering advection of both solid and fluid continue as time elapses. The meandering patterns are pronounced from $t = 2\ s$. The solid and fluid maxima are visible, particularly around the bends. Due to less amount of solid in the debris flood, the solid dynamics is more dominated and guided by fluid phase dynamics. Due to its lower density and lower material friction than the solid, fluid is more mobile. When compared to the solid phase's head at the same time slice, the fluid phase's head is situated substantially farther downstream. Their comparisons are also presented in Fig. 6. When the mass exits the conduits at $t = 5$ s, fluid has wider head but the solid has a sharper head due to the variation in their mobility. This indicates that the lateral spreading of fluid is higher than that of solid. When the flow exits the conduits, the lateral spreading of fluid causes the sudden decrease in flow depth as seen in the colour bar alongside.

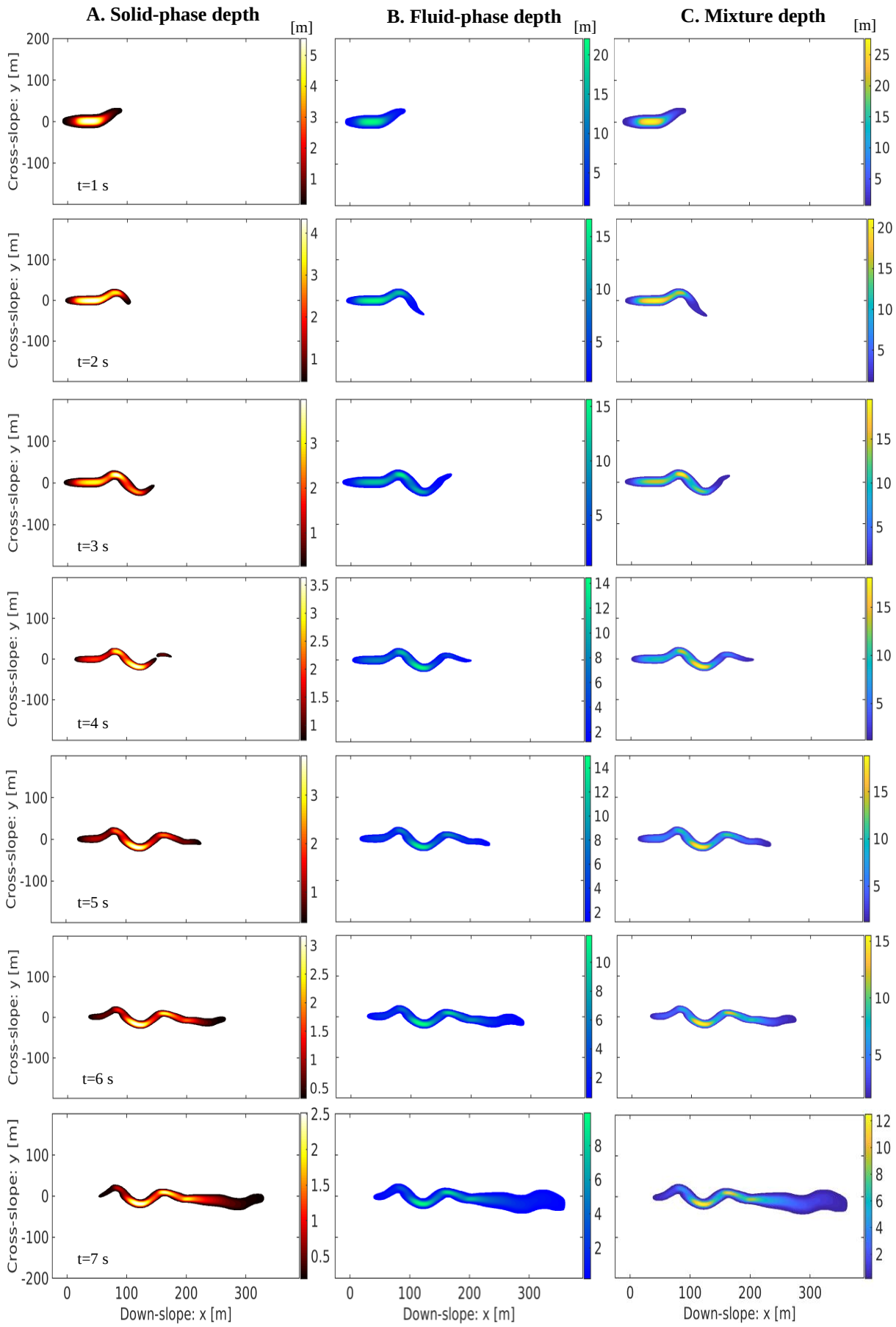

Fig. 5 Time and spatial evolution of the solid phase (panels A), fluid phase (panels B), and total debris (panels C) at t= 1, 2, 3, 4, 5, 6 and 7 s as the debris flood (0 m ≤ x ≤ 50 m) triggers down a sinuous channel (144 m ≤ x ≤ 200 m) with amplitude 15. Dispersed flow maxima are seen at the vicinity of the bends

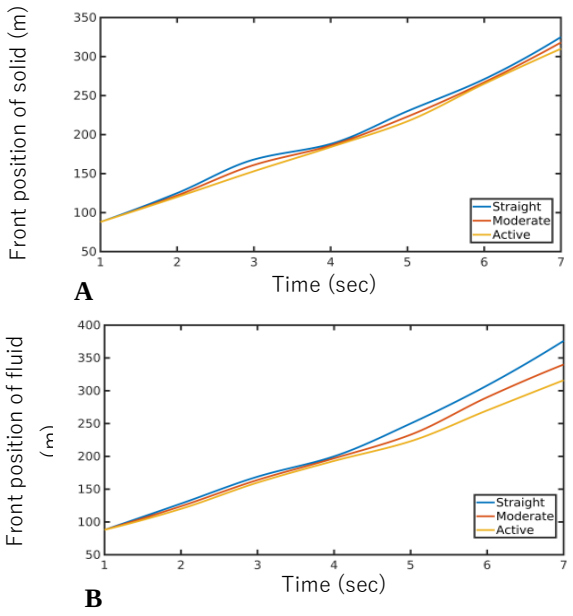

Fig. 6 A: Front positions of solid phase, B: fluid phase as the debris flood down straight, moderate and active sinuous conduits. The position of the front in each phase is at a bit backward as sinuosity increases

4.3 Debris Flood Down a Meandering Channel with Active Sinuosity

When amplitude of the meandering channel is increased to 30 m (Fig. 7), the distance from the bend to the middle horizontal line increases in comparison to that of amplitude 15 m (Fig. 5). Moreover, the increase in the amplitude also causes the increment in its sinuosity. When the amplitude was of 15 m (Fig. 5), the sinuosity was only 1.22 showing a moderate sinuousity. Amplitude of 30 m now increases the sinuosity to 1.69, indicating relatively more active meandering and the length of the course for the mass to flow is also increased in the meandering conduits within $50 \leq x \leq 200$ m. Evolution of the solid, fluid and mixture of the debris are exhibited in Fig. 6 in panels A, B and C respectively.

At time $t = 1$ s, the flood mixture starts to enter the meandering conduits. The increment in the amplitude causes increase of the river length where debris mass has to flow. As a result, the front of each of the phases is at a bit backward in comparison to the straight conduits (Fig. 4) and meandering conduits with lower amplitude of 15 m (Fig. 5). The dynamics of the flow due to greater sinuosity is more pronounced after $t = 2$ s where the flow path shows larger concavity and convexity as amplitude is increased. On the other hand, as soon as the mass starts to enter the sinuous curve, we can see the substantial differences in the dynamics compared to the prior simulations (Fig. 4, 5). The positions of the fronts are a bit back as the flow has to travel a longer conduit path as sinuosity is increased, especially after $t = 3$ s. The position of the fronts for different sinuosities are demonstrated in Fig. 6. At $t = 1$ s, the depths of the phases in all cases are almost similar but they are substantially different after $t = 2$ s. At $t = 2$ s, maxima of the mixture is at main body in straight channel with depth 25 m whereas there is elongated maxima with depth 20 m in moderate meandering. But in the active meandering, it is only 18 m as the maxima are separated in the rear, especially in the vicinity of the bends. At $t = 3$ s, the maxima are further separated around the bends. The maxima at the rear part indicate that there is still a significant amount of mass in the initial straight channel yet to flow. At $t = 7$ s, the position of the maximum is at the rear part with depth 6.5 m indicating that significant amount of mass is still obstructed at the back. Most of the studies of the debris flow/floods in meandering channels are carried out by considering a bulk mixture flow with channel migration (Darby et al., 2002; Motta et al., 2012), open-channel bends (Hu & Yu, 2023) and meander formations (Duan & Julien, 2005). In this study, we have revealed the time evolution of the separate solid and fluid phases and also the geometric evolution of the bulk mixture in pre-existing non-deformable straight and meandering conduits of two different sinuosities. Such two-phase studies will be useful to describe the different phase flow dynamics and phase separation.

5. CONCLUSION

Debris floods down meandering channels are commonly observed in nature. These floods consist of a mixture of solid and fluid and they may have substantial velocity differences due to different mechanics and rheology of the phases, having large influence on flow dynamics. For numerical experiments of these natural events in the meandering channel, we employed a two-phase depth-averaged model and demonstrated the evolution and dynamics of mixture flow along with the solid and fluid constituents separately. The numerical results presented here show that in the mixture of solid and fluid, fluid has greater velocity and hence larger mobility in downslope and cross-slope direction in comparison to the solid. As a result, the head of fluid phase is located farther downstream than that of the solid phase at the same instant. At the moment of the initial release, pressure gradient-induced reverse mass flow persists as there is no conduit at the rear part of the release mass. The results reveal that flowing mass tends to accumulate momentarily especially around the bends as sinuosity increases, which lowers the flow velocity and enables the mass to flow more slowly than it would in straight conduits or with conduits of lower sinuosity. The frontal head widens and spreads across as the flow starts to leave the conduits because lateral confinements are no longer there to obstruct the flow dispersion. The increase in the amplitude of sinuosity of the meandering lowers the flow velocity and increases the momentary deposition in the vicinity of the bends. This study suggests that channel flow can be slowed down by meandering, which has a significant effect on sedimentation. These studies can be applicable to study the dynamics of the natural gravitational flows of geophysical mass in already existing channels like in episodic rivers where debris flow or flood occurs suddenly due to heavy rain.

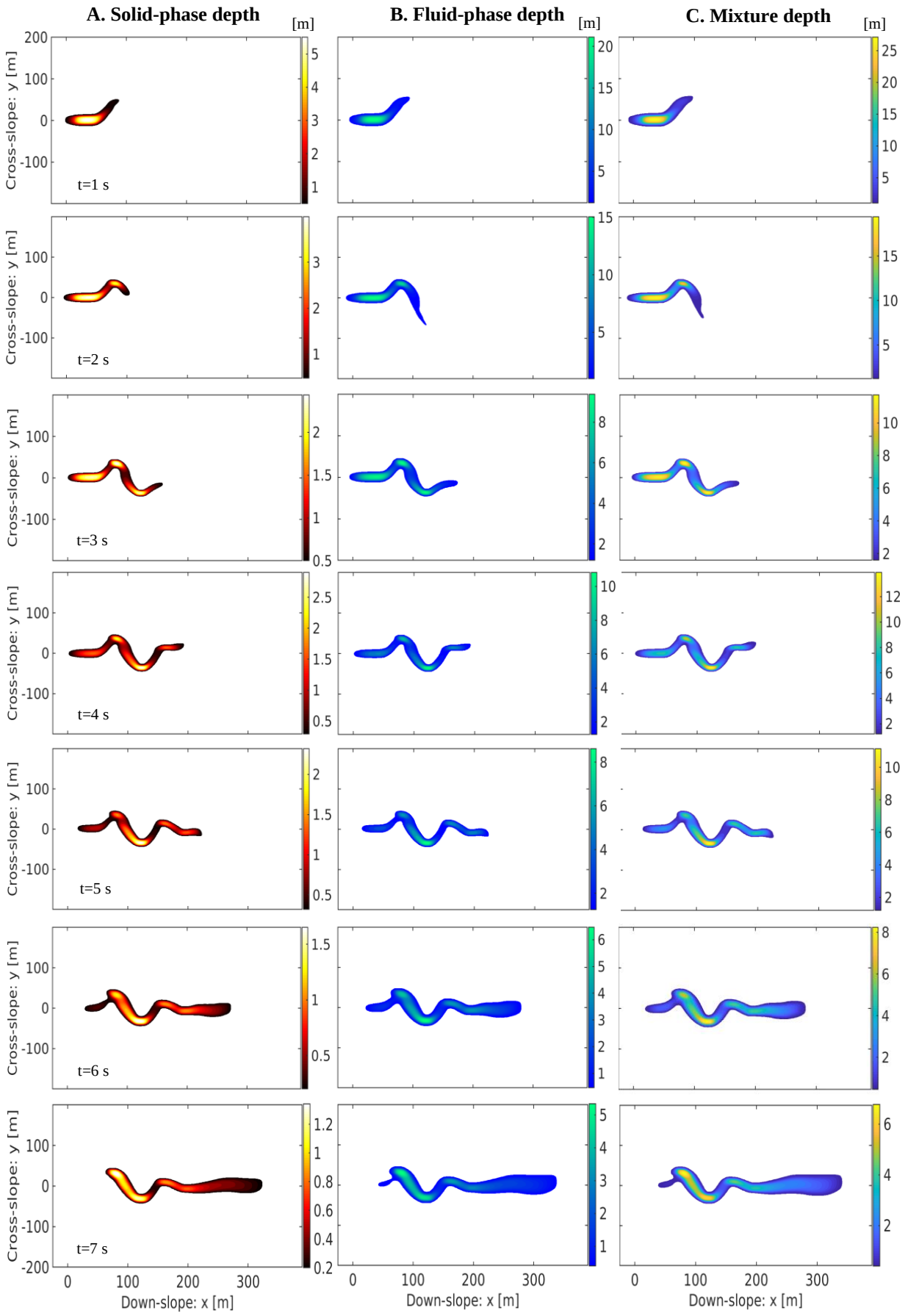

Fig. 7 Time and generic evolution of the solid phase (Left panels), fluid phase (Middle panels), and total debris (right panels) at t= 1,2,3,4,5,6 and 7s as the debris flood (0 m ≤ x ≤ 50 m) triggers down a sinuous channel (144 m ≤ x ≤ 200 m) with amplitude 30. Due to active meandering, maxima are seen at the rear part of the flowing mixture

ACKNOWLEDGEMENTS

Parameshwari Kattel acknowledges University Grants Commission (UGC), Nepal (Grant number: SRDIG-77/78-S. & T.-1). Chet Nath Tiwari and Bekha Ratna Dangol acknowledge the Research Directorate, Rector Office, Tribhuvan University, Kathmandu, Nepal for the grants with grant numbers 3-2078-2079 and 36-2078-2079 respectively. We also acknowledge the anonymous reviewers, editors, and the editor-in-chief for their careful review of the manuscript, providing valuable comments and insightful suggestions that significantly enhanced the manuscript.

CONFLICT OF INTEREST

There is no conflict of interest among the authors.

AUTHORS CONTRIBUTIONS

Parameshwari Kattel: Developed the idea, designed the research work and edited the manuscript. **Chet Nath Tiwari**: Contributed to the numerical experiments and initiated the draft of the manuscript. **Bekha Ratna Dangol**: Contributed to the analysis of the results and manuscript preparation. **Jeevan Kafle**: Contributed to the analysis of the results, discussion, and undertook the responsibility of correspondence with the Journal.

REFERENCES

Bagnold, R. A. (1954). Experiments on a gravity-free dispersion of large solid spheres in a Newtonian fluid under shear. *Proceeding of the Royal Society A, 225*, 49–63. https://doi.org/10.1098/rspa.1954.0186.

Bogoni, M., Putti, M., & Lanzoni, M. (2017). Modeling meander morphodynamics over self-formed heterogeneous floodplains. *Water*, *53*(6), 5137-5157. https://doi.org/ 10.1002/2017WR020726.

Camporeale, C., Perona, P., Porporato, A., & Ridolfi, L. (2002). On the long-term behavior of meandering rivers. *Water Resources Research*, *41*(12). https://doi.org/10.1029/2005WR004109.

Cassar, C., Nicolas, M., & Pouliquen, O. (2005). Submarine granular flows down inclined planes. *Physics of Fluids*, *17*, 103301. https://doi.org/ 10.1063/1.2069864.

Chen, C. L. (1988). Generalized viscoplastic modelling of debris flows. *Hydraulic Engineering*, *114*(3), 237–258. https://doi.org/10.1061/(ASCE)07339429(1988)114:3(237).

Coussot, P., & Ancey, C. (1999). Rheophysical classification of concentrated suspensions and granular pastes. *Physical Review E*, *59*(4), 4445–4457. https://doi.org/10.1103/PhysRevE.59.4445

Coussot, P., & Meunier, M. (1996). Recognition, classification and mechanical description of debris flows. *Earth-Science Reviews*, *40*(3-4), 209–227. https://doi.org/10.1016/00128252(95)00065-8.

Coz, J. L., Michalkova, M. S., Hauet, A., Comaj, M., Dramais, G., Holubova, K., Piegay, H., & Paquier, A. (2010). Morphodynamics of the exit of a cutoff meander: Experimental findings from field and laboratory studies. *Earth Surface Processes and Landforms*, *35*(3), 249–261. https://doi.org/ 10.1002/esp.1896.

Crosato, A. (2008). *Analysis and modelling of river meandering*. [PhD thesis, Delf University of Technology], Delf, Netherland.

Darby, S. E., Alabyan, A. M., & Wiel, M. J. V. D. (2002). Numerical simulation of bank erosion and channel migration in meandering rivers. *Water Resources Research*, *38*(9), 1163–1174. https://doi.org/10.1029/2001WR000602.

Delannay, R., Valance, A., Mangeney, A., Roche, O., & Richard, P., (2017). Granular and particle-laden flows: from laboratory experiments to field observations. *Journal of Physics D: Applied Physics*, *50*(5). https://doi.org/10.1088/13616463/50/5/053001.

Dente, E., Lensky, N., Morin, E., & Enzel, Y. (2021). From straight to deeply incised meandering channels: Slope impact on sinuosity of confined streams. *Earth Surface Processes and Landform*, *46*(563), 1041-1055. https://doi.org/10.1002/esp.5085.

Duan, J. G., & Julien, P. Y. (2005). Numerical simulation of meandering evolution. *Journal of Hydrology*, *391*(1-2), 34-46. https://doi.org/10.1016/j.jhydrol.2010.07.005.

Duan, J. G. (2004). Simulation of flow and mass dispersion in meandering channels. *Hydraulic Engineering*, *130*(10), 964–976. https://doi.org/10.1061/(ASCE)0733-9429(2004)130:10(964).

Friedkin, J. F. (1945). A laboratory study of the meandering of alluvial rivers. *Engineers Waterways Experiment Stations*.

Gu, L., Zhang, S., He, L., Chen, D. Blanckaert, K., Ottevanger, W., & Zhang, Y. (2016). Modeling flow pattern and evolution of meandering channels with a nonlinear model. *Water*, *8*(10). https://doi.org/10.3390/w8100418.

Hagerman, J. R., & Williams J. D. (2000). Meander shape and the designs of stable meanders. *Agricultural Research Service*.

Hu, P., & Yu, M. (2023). Experimental study of secondary flow in narrow and sharp open channels bends. *Journal of Applied fluid Mechanics*, *16*(9). https://doi.org/10.47176/JAFM.16.09.1672

Ikeda, S., & Nishimura, T. (1986). Flow and bed profile in meandering sand-silt rivers. *Hydraulic Engineering*, *112*(7), 562–579. https://doi.org/10.1061/(ASCE)07339429(1986)112:

7(562).

Iverson, R. M. (1997). The physics of debris flows. *Reviews of Geophysics*, *35*(3), 245–296. https://doi.org/10.1029/97RG00426.

Iverson, R. M. (2003). *The debris-flow rheology myth*. Presented at the 3rd International Conference on Debris-Flow Hazards Mitigation: Mechanics, Prediction, and Assessment.

Iverson, R. M., & George, D. L. (2014). A depth-averaged debris-flow model that includes the effects of evolving dilatancy. *I.* Physical basis. *Proceeding of Royal Society A*, 470, 20130819. https://doi.org/10.1098/rspa.2013.0819.

Kafle, J., Acharya, G., Kattel, P., & Pokhrel P. R. (2022). Impact of variation of size of the initial release mass in the dynamics of landslide generated tsunami. *International Journal of Modeling, Simulation, and Scientific Computing*, *13*(5), 217–225. https://doi.org/10.1142/S1793962322500556.

Kafle, J., Dangol, B. R., Tiwari, C. N., & Kattel, P. (2023). Dynamics of landslide-generated tsunamis and their dependence on the particle concentration of initial release mass. *European Journal of Mechanics - B/Fluids*, *97*, 146–161. https://doi.org/10.1016/j.euromechflu.2022.10.003.

Kafle, J., Kattel, P., Pokhrel, P. R., & Khattri, K. B. (2021). Numerical experiments on effect of topographical slope changes in the dynamics of landslides generated water waves and submarine mass flows. *Journal of Applied Fluid Mechanics*, *14*(3), 861-876. https://doi.org/10.47176/jafm.14.03.31740

Kafle, J., Pokhrel, P. R. Khattri, K. B., Kattel, P., Tuladhar, B. M., & Pudasaini, S. P. (2016). Submarine landslide and particle transport in mountain lakes, reservoirs and hydraulic plants. *Annals of Glaciology*, *57*(71), 232– 244. https://doi.org/10.3189/2016AoG71A034.

Kattel, P., & Tuladhar, B. M. (2018). Interaction of two-phase debris flow with lateral converging shear walls. *Journal of Nepal Mathematical Society*, 1(2), 40–52. https://doi.org/10.3126/jnms.v1i2.41490.

Kattel, P., Kafle, J., Fischer, J.-T. Mergili, M. Tuladhar, B. M., & Pudasaini, S. P. (2018). Interaction of two-phase debris flow with obstacles. *Engineering Geology*, *242*, 197–217. https://doi.org/10.1016/j.enggeo.2018.05.023.

Kattel, P., Khattri, K. B. & Pudasaini, S. P. (2021). A multiphase virtual mass model for debris flow. *International Journal of Non-Linear Mechanics*, 129. https://doi.org/10.1016/j.ijnonlinmec.2020.103638.

Kattel, P., Khattri, K. B., Pokhrel, P. R., Kafle, J., Tuladhar, B. M., & Pudasaini, S. P. (2016). Simulating glacial lakea two-phase mass flow model. *Annals of Glaciology*, *57*(71), 349–358. https://doi.org/10.3189/2016AoG71A039.

Kinoshita, R. (1961). An investigation of channel deformation in Ishikari river. Science and Technology Agency, *Bureau of Resources*.

Kopera, K. N. (2014). Identifying the distinct rock types in the streambed of muddy run. *The Juniata Journal of Geology, 1*, 1–7.

Langbein, W. B., & Leopold, L. B. (1966). *River meanders – Theory of minimum variance.* Geological Survey Professional Paper 422-H. United States Government Printing Office, Washington, D. C. https://doi.org/10.3133/pp422H.

Leopold, L. B. & Wolman, M. G. (1960). River meanders. *Geological Society of America*, 71(6), 769–793. https://doi.org/10.1130/00167606(1960)71[769:RM]2.0.CO;2.

Mohamad, I. N., Lee, W. K., & Raksmey, M. (2015). *Idealized river meander using improved sine-generated curve method.* International Civil & Infrastructure Engineering Conference. https://doi.org/10.1007/978-981-10-0155-0_13.

Montgomery, D. R. & Buffington, J. M. (1998). Channel processes, classification and response. In R. Naiman & R. Bilby (Eds.), *River Ecology and Management*, Springer-Verilog, New York.

Motta, D., Abad, J. D., Langendoen, E. J., & Garcia, M. H. (2012). A simplified 2-d model for meander migration with physically based bank evolution. *Geomorphology*, *163-164*, 10–25. https://doi.org/10.1016/j.geomorph.2011.06.036.

Murray, A. B., & Paola, C. (1994). A cellular model of braided rivers. *Nature*, *371*(6492), 54–57. https://doi.org/10.1038/371054a0.

Parker, G., Diplas, P., & Akiyama, J. (1983). Meander bends of high amplitude. *Journal of Hydraulic Engineering*, *109*(10), 1323–1337. https://doi.org/10.1061/(ASCE)0733-9429(1983)109:10(1323).

Pastor, M., Yague, A., Stickle, M.M., Manzanal, D., & Mira, P. (2018). A two-phase SPH model for debris flow propagation. *International Journal of Numerical and Analytical Methods in Geomechanics*, *42*(4), 418–448. https://doi.org/10.1002/nag.2748.

Pierson, T. C. (2005a). *Hyperconcentrated flow - transitional process between water flow and debris flow, in: Jakob, M., Hungr, O. (Eds.), Debris-Flow Hazards and Related Phenomena*, (pp. 159-202) Springer Praxis, Berlin, Heidelberg. https://doi.org/10.1007/3-540-27129-5_8.

Pierson, T. C. (2005b). *Distinguishing between debris flows and floods for field evidence in small watersheds*. U.S. Geological Survey Fact Sheet, 2004-3142. https://doi.org/10.3133/fs20043142.

Pudasaini, S. P. & Krautblatter, M. (2014). A two-phase mechanical model for rock-ice avalanches. *JGR Earth Surface*, *119*(10), 2272–2290,

https://doi.org/10.1002/2014JF003183.

Pudasaini, S. P. (2012). A general two-phase debris flow model. *Journal of Geophysical Research, 117*(F3) 3010. https://doi.org/10.1029/2011JF002186.

Rozovskii, I. L. (1957). *Flow of water in bends of open channels.* Academy of Sciences of the Ukrainian SSR, Israel Program for Scientific Translation.

Stolum, H. H. (1996) Landslide tsunamis propagating along the plane beach. *Science, 271*, 1710-1713.

Tai, Y. C., Noelle, S., Gray, J. M. N. T., & Hutter, K. (2002). Shock- capturing and front-tracking methods for granular avalanches. *Journal of Computational Physics, 175*, 269-301. https://doi.org/10.1006/jcph.2001.6946.

Takahasi, T. (2007). *Debris flow: Mechanics, prediction and counter measures.* Taylor and Francis, New York.

Tulapurkara, E. G., Gowda, B. H. L., & Swain, S. K. (1994). Reverse flow in channel-effect of front and rear obstructions. *Physics of Fluids, 6*(12), 3847–3853. https://doi.org/10.1063/1.868376.

Wilford, D., Sakals, M. E., Innes, J. L., Sidle, R. & Bergerud, W. A. (2004). Recognition of debris flow, debris flood and flood hazard through watershed morphometrics. *Landslides, 1*(1), 61–66. https://doi.org/ 10.1007/s10346-003-0002-0.

Yong, N. S., Mohamad, I. N., & Lee, W. K. (2018). Experimental study on river meandering planform pattern. International *Journal of Engineering & Technology, 7*(11), 214-217. https://doi.org/10.14419/ijet.v7i3.11.15965.

Zimmerman, C., & Kennedy, J. F. (1978). Transverse bed slopes in curved alluvial. *ASCE Journal of Hydraulic Division, 104*(1), 33-48. https://doi.org/10.1061/JYCEAJ.0004922.